Universal Dynamical Decoupling of a Single Solid-State Spin from a Spin Bath

G. de Lange, *et al.*

Science **330**, 60 (2010);
DOI: 10.1126/science.1192739

proper expression or for modulating channel properties, similar to β subunits of voltage-gated channels (*32*) or SUR subunits of adenosine 5′-triphosphate–sensitive K+ channels (*33*). In this case, all the cell types used here would have to express an inactive conducting subunit of an MA channel that requires Piezos to function. Alternatively, Piezo proteins may define a distinct class of ion channels, akin to Orai1, which lacks sequence homology to other channels (*34*). Piezo1 is also found in the endoplasmic reticulum (*14*, *15*), so Piezos may act at both the plasma membrane and in intracellular compartments.

We described a role of Piezo2 in rapidly adapting MA currents in somatosensory neurons. Thus, Piezo2 has potential roles in touch and pain sensation (*35*, *36*). Piezo1 and Piezo2 are expressed in various tissues, and their homologs are present throughout animals, plants, and protozoa, raising the possibility that Piezo proteins have a broad role in mechanotransduction.

References and Notes

1. M. Chalfie, *Nat. Rev. Mol. Cell Biol.* **10**, 44 (2009).
2. O. P. Hamill, B. Martinac, *Physiol. Rev.* **81**, 685 (2001).
3. G. B. Monshausen, S. Gilroy, *Trends Cell Biol.* **19**, 228 (2009).
4. K. Iwatsuki, T. Hirano, *Comp. Biochem. Physiol. Physiol.* **110**, 167 (1995).
5. D. P. Corey, A. J. Hudspeth, *Biophys. J.* **26**, 499 (1979).
6. G. C. McCarter, D. B. Reichling, J. D. Levine, *Neurosci. Lett.* **273**, 179 (1999).
7. H. A. Praetorius, K. R. Spring, *J. Membr. Biol.* **184**, 71 (2001).
8. B. Coste, M. Crest, P. Delmas, *J. Gen. Physiol.* **129**, 57 (2007).
9. L. J. Drew, J. N. Wood, P. Cesare, *J. Neurosci.* **22**, RC228 (2002).
10. S. R. Besch, T. Suchyna, F. Sachs, *Pflugers Arch.* **445**, 161 (2002).
11. H. Cho *et al.*, *Eur. J. Neurosci.* **23**, 2543 (2006).
12. S. Earley, B. J. Waldron, J. E. Brayden, *Circ. Res.* **95**, 922 (2004).
13. R. Sharif-Naeini *et al.*, *Cell* **139**, 587 (2009).
14. K. Satoh *et al.*, *Brain Res.* **1108**, 19 (2006).
15. B. J. McHugh *et al.*, *J. Cell Sci.* **123**, 51 (2010).
16. R. O. Hynes, *Cell* **110**, 673 (2002).
17. G. Burnstock, *Mol. Pain* **5**, 69 (2009).
18. L. Rodat-Despoix, P. Delmas, *Pflugers Arch.* **458**, 179 (2009).
19. J. Hu, G. R. Lewin, *J. Physiol.* **577**, 815 (2006).
20. L. J. Drew *et al.*, *J. Physiol.* **556**, 691 (2004).
21. L. J. Drew *et al.*, *PLoS ONE* **2**, e515 (2007).
22. C. Wetzel *et al.*, *Nature* **445**, 206 (2007).
23. J. Hao *et al.*, in *Mechanosensitivity of the Nervous System*, I. K. e. A. Kamkin, Ed. (Springer Netherlands, 2008), vol. 2, pp. 51–67.
24. M. Schmidt, A. E. Dubin, M. J. Petrus, T. J. Earley, A. Patapoutian, *Neuron* **64**, 498 (2009).
25. Materials and methods are available as supporting material on *Science* Online.
26. M. E. Goldstein, S. B. House, H. Gainer, *J. Neurosci. Res.* **30**, 92 (1991).
27. S. N. Lawson, *Exp. Physiol.* **87**, 239 (2002).
28. S. N. Lawson, A. A. Harper, E. I. Harper, J. A. Garson, B. H. Anderton, *J. Comp. Neurol.* **228**, 263 (1984).
29. H. Sann, P. W. McCarthy, G. Jancsó, F. K. Pierau, *Cell Tissue Res.* **282**, 155 (1995).
30. M. Bandell *et al.*, *Neuron* **41**, 849 (2004).
31. S. E. Jordt *et al.*, *Nature* **427**, 260 (2004).
32. M. R. Hanlon, B. A. Wallace, *Biochemistry* **41**, 2886 (2002).
33. S. J. Tucker, F. M. Ashcroft, *Curr. Opin. Neurobiol.* **8**, 316 (1998).
34. M. Prakriya *et al.*, *Nature* **443**, 230 (2006).
35. A. I. Basbaum, D. M. Bautista, G. Scherrer, D. Julius, *Cell* **139**, 267 (2009).
36. G. R. Lewin, R. Moshourab, *J. Neurobiol.* **61**, 30 (2004).

37. The authors gratefully acknowledge H. Hu for help in cloning Piezo2, J. Walker for contributing to microarray experiments, S. Batalov for help in bioinformatics analysis, K. Spencer for help with imaging, and N. Hong and U. Müller for comments on the manuscript and helpful discussions. This work was supported by grants from NIH (DE016927 and NS046303) and the Novartis Research Foundation. B.C. is the recipient of an American Heart Association postdoctoral fellowship; M.S. is the recipient of a German Academic Exchange Service (DAAD, D/07/41089) fellowship. A provisional patent has been filed by TSRI and GNF that claims methods of screening for molecules that modulate Piezo-dependent ion channel activities. The Piezo1 and Piezo2 sequences used in the paper have been deposited in GenBank under accession numbers HQ215520 and HQ215521, respectively.

Supporting Online Material

www.sciencemag.org/cgi/content/full/science.1193270/DC1
Materials and Methods
Figs. S1 to S8
Tables S1 and S2
References

4 June 2010; accepted 20 August 2010
Published online 2 September 2010;
10.1126/science.1193270
Include this information when citing this paper.

REPORTS

Universal Dynamical Decoupling of a Single Solid-State Spin from a Spin Bath

G. de Lange,[1] Z. H. Wang,[2] D. Ristè,[1] V. V. Dobrovitski,[2] R. Hanson[1]*

Controlling the interaction of a single quantum system with its environment is a fundamental challenge in quantum science and technology. We strongly suppressed the coupling of a single spin in diamond with the surrounding spin bath by using double-axis dynamical decoupling. The coherence was preserved for arbitrary quantum states, as verified by quantum process tomography. The resulting coherence time enhancement followed a general scaling with the number of decoupling pulses. No limit was observed for the decoupling action up to 136 pulses, for which the coherence time was enhanced more than 25 times compared to that obtained with spin echo. These results uncover a new regime for experimental quantum science and allow us to overcome a major hurdle for implementing quantum information protocols.

In the past decade, manipulation and measurement of single quantum systems in the solid state have been achieved (*1*, *2*). This control has promising applications in quantum information processing (*3*, *4*), quantum communication (*5*), metrology (*6*), and ultrasensitive magnetometry (*7*, *8*). However, uncontrolled interactions with the surroundings inevitably lead to decoherence of the quantum states (*9*) and pose a major hurdle for realizing these technologies. Therefore, the key challenge in current experimental quantum science is to protect individual quantum states from decoherence by their solid-state environment.

If a quantum system can be controlled with high fidelity, dynamical decoupling can be exploited to efficiently mitigate the interactions with the environment (*10*–*12*). By reversing the evolution of the quantum system at specific times with control pulses, the effect of the environment accumulated before the pulse is canceled during the evolution after the pulse. When viewed at the end of the control cycle, the quantum system will appear as an isolated system that is decoupled from its environment. Thanks to recent progress in quantum control speed and precision (*13*, *14*), we can now unlock the full power of dynamical decoupling at the level of a single spin.

We focused on electron spins of single nitrogen-vacancy (NV) defect centers in diamond coupled to a spin bath (Fig. 1A). NV center spins can be optically imaged, initialized, and read out, as well as coherently controlled at room temperature (Fig. 1B). These favorable properties have been exploited to gain deeper insight into spin decoherence (*15*, *16*), as well as for demonstrating basic quantum information protocols at room temperature (*17*, *18*).

We used nanosecond microwave pulses to manipulate single NV spins. To raise the fidelity of our control to the required level for efficient decoupling, we fabricated on-chip coplanar waveguide (CPW) transmission lines using electron beam lithography (Fig. 1A). The high bandwidth of the CPW (*13*) combined with efficient suppression of reflections and fine-tuned pulse calibration (*14*) allows fast and precise manipulation of

[1]Kavli Institute of Nanoscience Delft, Delft University of Technology, Post Office Box 5046, 2600 GA Delft, Netherlands. [2]Ames Laboratory and Iowa State University, Ames, IA 50011, USA.

*To whom correspondence should be addressed. E-mail: r.hanson@tudelft.nl

the NV spin (Fig. 1B), leading to process fidelities of 99% for the basic control pulses needed for dynamical decoupling (*14*).

The coherent dynamics of an NV spin are strongly influenced by the coupling to neighboring spins (the spin bath) (*15*, *16*). Because such spin environments are common in the solid state, our results are directly relevant for other solid-state quantum bits such as spins in quantum dots (*19*, *20*) and donors in silicon (*4*, *21*). For the NV centers studied here, the bath is composed of electron spins localized on nitrogen impurity atoms. Resonant interactions (flip-flops) between the bath spins and the NV spin are suppressed because of a large energy mismatch (*16*). Therefore, the impact of the spin bath on the NV spin is limited to dephasing and can be described as a random magnetic field $B(t)$ that is directed along the NV's quantization axis. The value of $B(t)$ is determined by the state of the environment. We modeled the bath field $B(t)$ by an Ornstein-Uhlenbeck process with the correlation function $C(t) = \langle B(0)B(t)\rangle = b^2 \exp(-|t|/\tau_C)$, where b is the coupling strength of the bath to the spin and τ_C is the correlation time of the bath, which measures the rate of flip-flops between the bath spins due to the intrabath dipolar coupling (*14*, *22*).

The values of the parameters describing the bath field were extracted from experiments. The bath-induced dephasing during free evolution had a Gaussian envelope $S(t) = \exp(-b^2t^2/2)$, which yielded the value for b (*14*); we found $b = (3.6 \pm 0.1)\ \mu s^{-1}$ for NV1 (Fig. 1C), and $b = (2.6 \pm 0.1)\ \mu s^{-1}$ for NV2 (*14*). The quasi-static dephasing could be undone with a spin echo (SE) technique (Fig. 2A), revealing the much slower decay of spin coherence caused by the dynamics of the spin bath. The spin echo signal decayed as $SE(t) = \exp[-(t/T_2)^3]$, characteristic for a slowly fluctuating spin bath with $\tau_C = T_2^3 b^2/12 >> 1/b$ (*22*). The values we found for τ_C, $(25 \pm 3)\ \mu s$ for NV1 [$T_2 = (2.8 \pm 0.1)\ \mu s$] and $(23 \pm 3)\ \mu s$ for NV2 [$T_2 = (3.5 \pm 0.2)\ \mu s$], confirmed this. The spin echo decay time T_2 is often considered as the coherence or memory time of the system. We took T_2 as the starting point and demonstrated that the coherence time could be markedly prolonged by dynamically decoupling the spin from the surrounding spin bath.

We first explored the potential of dynamical decoupling by extending the SE pulse sequence to periodic repetitions of the Carr-Purcell-Meiboom-Gill (CPMG) cycle (Fig. 2A). The decoupling performance was characterized by measuring the state fidelity $F_s = \langle\psi_i|\rho_m|\psi_i\rangle$, where $|\psi_i\rangle$ is the expected (ideal) state after applying the sequence and ρ_m the measured density matrix of the actual state. Although the coherence had vanished after 4 μs for the SE case, we observed that the eight-pulse CPMG sequence preserved the coherence almost completely during this same time.

The optimal decoupling sequence for a quantum system depends on the coupling to its environment and the dynamics within the environment itself. In (*23*), nonperiodic interpulse spacing, now called the UDD sequence, was found to achieve a strong improvement in decoupling efficiency over periodic pulse spacing in the case of environmental noise spectra with a hard cutoff; this was experimentally verified in (*24*, *25*). Recent theory (*26*, *27*), however, suggests that periodic, CPMG-like pulse spacing is ideal for decoupling from an environment with a soft cut-

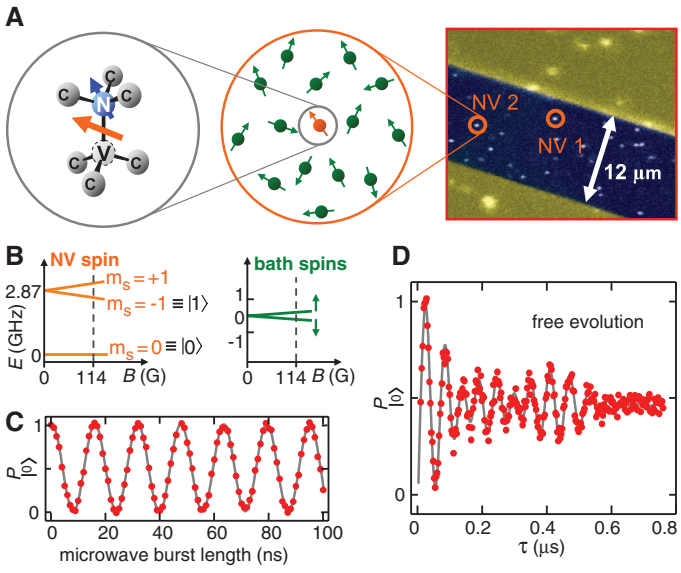

Fig. 1. Quantum control of a single spin in diamond. (**A**) Left: A nitrogen-vacancy defect is formed by a single substitutional nitrogen (^{14}N) atom and an adjacent vacancy (V). The NV electron spin (orange arrow) is coupled to the host ^{14}N nuclear spin (blue arrow) through the hyperfine interaction. Middle: The NV center is surrounded by a bath of electron spins located at sites of substitutional nitrogen atoms in the diamond lattice (*16*). Right: Confocal photoluminescence scan of a section of the device, where the golden regions are part of the on-chip coplanar waveguide (CPW) used for applying quantum control pulses and NV centers appear as bright spots in between the conductors of the CPW. (**B**) Energy level diagrams of the NV center electron spin (left) and the electron spins in the bath (right). An applied magnetic field splits the NV spin triplet electronic ground state; the effective two-level system used here is formed by the spin sublevels $m_S = 0$ (labeled $|0\rangle$) and $m_S = -1$ (labeled $|1\rangle$) (*14*). (**C**) Coherent driven oscillations of NV1. For the pulsed experiments, the same Rabi frequency is used (*14*). (**D**) Decay during free evolution of NV1 probed using Ramsey interference. Solid line is a fit (*14*). The fast oscillating component is due to a detuning of the driving field of 15 MHz with respect to the spin transition, whereas the beating is caused by the hyperfine interaction with the host nuclear spin.

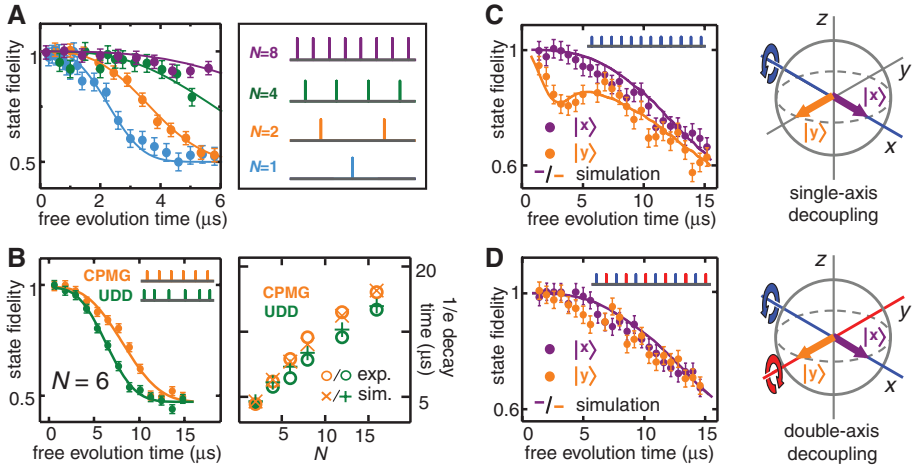

Fig. 2. Optimized dynamical decoupling of NV1. (**A**) Left: State fidelities for CPMG decoupling sequence applied to NV1. The blue curve is a spin echo measurement. High state fidelity is recovered for increasing number of pulses N. Solid lines are fits to $\sim\exp[-(t/T_{coh})^3]$. Right: Vertical lines indicate the location of π-pulses. (**B**) Comparison of decoupling with CPMG (orange) and UDD (green) for $N = 6$ pulses. The solid lines are fits to $\sim\exp[-(t/T_{coh})^3]$. The right panel shows the $1/e$ decay times from fits to data and to simulations (*14*). The same color scheme applies. (**C**) Single-axis decoupling for different input states, showing state-selective decoupling for the CPMG sequence with $N = 12$ operations (shown in the upper right). Bloch sphere on the right shows input states and the decoupling axis. Solid lines are numerical simulations incorporating the experimental pulse errors (*14*). (**D**) Double-axis decoupling, with XY4 sequence with $N = 12$, showing excellent decoupling for both input states. Pulse timings are the same as for CPMG but with the decoupling axis alternating between X and Y, as shown on the right. The simulations for $|x\rangle$ and $|y\rangle$ yield practically the same curve and therefore appear as one.

off. We investigated the efficiency of these different protocols in decoupling a single spin from a spin bath environment (Fig. 2B) and observed that CPMG outperformed UDD for all numbers of pulses investigated in both simulations and experiments (Fig. 2B, right panel). These findings are in agreement with our model of a Lorentzian bath noise spectrum, which exhibits a soft cut-off (*14*).

For applications in quantum information processing, it is essential that the decoupling protocol is universal, meaning that it can preserve coherence for arbitrary quantum states. Because pulse errors can severely degrade the coherence, universal decoupling requires robustness to pulse errors for all possible quantum states. In contrast, protocols that use single-axis decoupling such as CPMG optimally preserve only a limited range of quantum states, whereas for other quantum states the pulse errors accumulate rapidly with increasing number of control pulses. In Fig. 2C, we demonstrated this experimentally by comparing the decay curves of superposition states aligned ($|x\rangle$) and perpendicular ($|y\rangle$) to the CPMG decoupling axis. Even though the fidelity of the single-pulse control was very high (*14*), the remaining small errors caused a significant loss of decoupling fidelity for state $|y\rangle$ when the number of operations was increased to 12 pulses; this effect was accurately reproduced by simulations (Fig. 2C) (*14*).

The use of sequences containing decoupling pulses over two axes, such as XY4 (Fig. 2D) (*28*), avoids this selective robustness to pulse errors and can compensate certain systematic pulse errors and coherent resonant perturbations without increasing control overhead. We found that XY4 could indeed preserve both quantum states $|x\rangle$ and $|y\rangle$ (Fig. 2D).

We studied the decoupling performance in more detail with the use of quantum process tomography (QPT), which allows for a complete characterization of any quantum process (*29*). Figure 3 shows the experimental QPT results for XY4 with $N = 8$ operations, at different free evolution times. For a free evolution time of 4.4 μs, much longer than T_2, the measured process matrix χ is in excellent agreement with the ideal process of identity that is expected for perfect universal decoupling.

By taking snapshots of the process for different free evolution times, we monitored how decoherence affects the quantum states. We observed that after $t = 10$ μs, the process element corresponding to identity had decreased, whereas the σ_z-σ_z element had grown. After 20 μs, these elements had approximately equal amplitudes. This behavior is characteristic for pure, off-diagonal dephasing (*29*) and is consistent with our model of the environment, in which the magnetic dipolar coupling with the bath leads to phase randomization. The independently measured energy relaxation time $T_1 > 1$ ms (*14*) confirmed that longitudinal decay is not relevant in this regime.

Finally, we investigated how the coherence time scales with the number of control pulses. A detailed theoretical analysis showed that for N perfect pulses, the decoupling fidelity decayed as $F(t) = \exp[-ANt^3/(2N\tau_C)^3]$, where the total free evolution time $t = 2N\tau$ and 2τ is the interpulse distance (*14*). For the XY4 sequence, we found that $A = (2/3)b^2\tau_C^2$ for both large and small N. The theory predicts two interesting features: (i) The decay follows the universal form $\exp[-(t/T_{coh})^3]$ for all N, and (ii) the $1/e$ decay time scales as $T_{coh}(N) = T_2 N^{2/3}$.

In Fig. 4A, we show XY4 decoupling for $N = 4$, 16, and 72, as well as the spin echo for comparison. These data indicate that the $1/e$ decay time indeed scales with the number of pulses. For a thorough comparison with the theory, we renormalized the time axis to $T_2 N^{2/3}$ (Fig. 4B). We found that all data collapse onto a single curve in line with the prediction. Then, we plotted the $1/e$ decay time of coherence of NV1 and NV2 and fit this to the expected scaling law. The data of both NV centers showed excellent agreement with the theory over a range in N spanning two orders of magnitude. For the longest sequence applied (136 pulses), the coherence time was increased by a factor of 26.

Is there a limit to the coherence enhancement that can be achieved with dynamical decoupling? Our results demonstrate that we can prolong the spin coherence beyond the bath correlation time τ_C. Also, the nuclear spin bath, which would affect the NV dynamics on a 5-μs time scale for the magnetic field used here (*15*), is efficiently decoupled from the NV spin. Indeed, the theory indicates no fundamental limit to the coherence time. In practice, the decoupling efficiency will be limited by the minimum interpulse delay (on the order of the pulse widths) and the longitudinal relaxation time.

Because the spin bath environment is common to solid-state quantum bits, our findings can be transferred to other promising systems such as spins in quantum dots (*3*, *19*, *20*) and donors in silicon (*4*, *21*). Furthermore, the performance of spin-based magnetometers can greatly benefit from this work, because the magnetic field sensitivity scales with the coherence time (*7*, *8*). Fi-

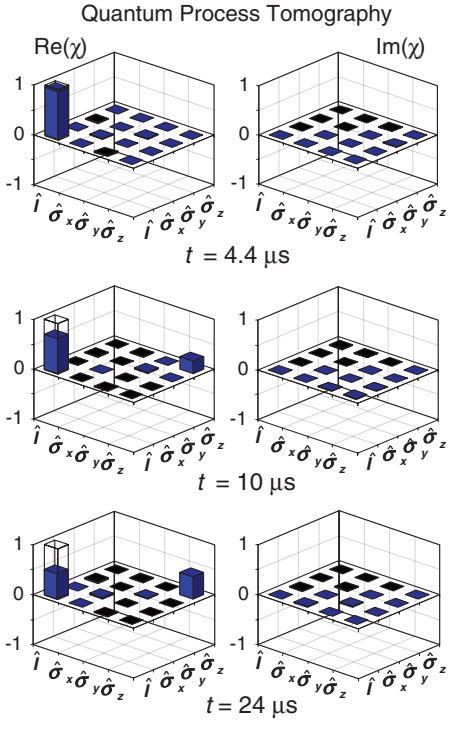

Fig. 3. Universal decoupling demonstrated with quantum process tomography. QPT is performed at free evolution times of 4.4, 10, and 24 μs for XY4 with $N = 8$ (see fig. S2B). At $t = 4.4$ μs, the measured process matrix nearly equals the identity process matrix χ (fidelity of 0.96 ± 0.02), indicating close-to-perfect quantum state protection. At longer free evolution times, the process changes into pure dephasing in accordance with our model of the spin bath.

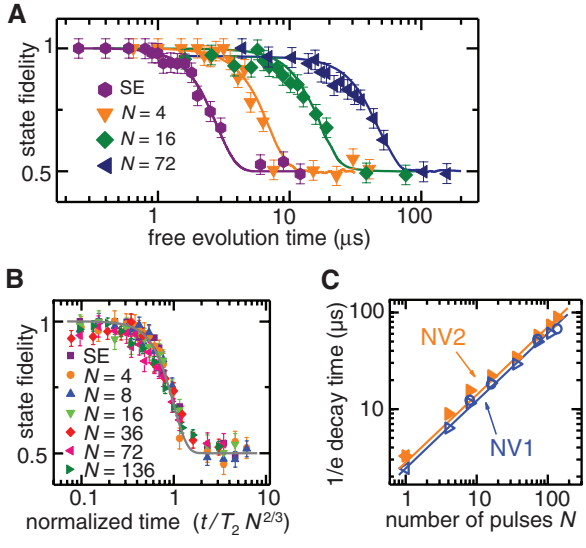

Fig. 4. Scaling of the coherence enhancement with number of control pulses. (**A**) Decoupling for different number of control pulses N. Increasing N extends the coherence to longer times. Solid lines are simulations (*14*). (**B**) Data rescaled to the normalized time axis $t/(T_2 N^{2/3})$. (**C**) Coherence $1/e$ decay time (T_{coh}) plotted as a function of the number of control pulses for NV1 and NV2. Solid lines are fits to $T_{coh}(N) = T_2 N^{2/3}$ with T_2 as free parameter.

nally, dynamical decoupling can be applied to protect entangled states, which are at the heart of quantum information science.

References and Notes

1. J. Clarke, F. K. Wilhelm, *Nature* **453**, 1031 (2008).
2. R. Hanson, D. D. Awschalom, *Nature* **453**, 1043 (2008).
3. D. Loss, D. P. DiVincenzo, *Phys. Rev. A* **57**, 120 (1998).
4. B. E. Kane, *Nature* **393**, 133 (1998).
5. L. Childress, J. M. Taylor, A. S. Sørensen, M. D. Lukin, *Phys. Rev. Lett.* **96**, 070504 (2006).
6. J. A. Jones *et al.*, *Science* **324**, 1166 (2009).
7. C. Degen, *Appl. Phys. Lett.* **92**, 243111 (2008).
8. J. M. Taylor *et al.*, *Nat. Phys.* **4**, 810 (2008).
9. W. H. Zurek, *Nat. Phys.* **5**, 181 (2009).
10. L. Viola, L. Knill, S. Lloyd, *Phys. Rev. Lett.* **82**, 2417 (1999).
11. D. Vitali, P. Tombesi, *Phys. Rev. A* **59**, 4178 (1999).
12. K. Khodjasteh, D. A. Lidar, *Phys. Rev. Lett.* **95**, 180501 (2005).
13. G. D. Fuchs, V. V. Dobrovitski, D. M. Toyli, F. J. Heremans, D. D. Awschalom, *Science* **326**, 1520 (2009).
14. Materials and methods are available as supporting material on *Science* Online.
15. L. Childress *et al.*, *Science* **314**, 281 (2006).
16. R. Hanson, V. V. Dobrovitski, A. E. Feiguin, O. Gywat, *Science* **320**, 352 (2008).
17. L. Jiang *et al.*, *Science* **326**, 267 (2009).
18. P. Neumann *et al.*, *Nat. Phys.* **6**, 249 (2010).
19. R. Hanson, L. P. Kouwenhoven, J. R. Petta, S. Tarucha, L. M. K. Vandersypen, *Rev. Mod. Phys.* **79**, 1217 (2007).
20. H. Bluhm *et al.*, http://arxiv.org/abs/1005.2995v1 (2010).
21. J. J. L. Morton *et al.*, *Nature* **455**, 1085 (2008).
22. J. Klauder, P. Anderson, *Phys. Rev.* **125**, 912 (1962).
23. G. S. Uhrig, *Phys. Rev. Lett.* **98**, 100504 (2007).
24. M. J. Biercuk *et al.*, *Nature* **458**, 996 (2009).
25. J. Du *et al.*, *Nature* **461**, 1265 (2009).
26. S. Pasini, G. S. Uhrig, *Phys. Rev. A* **81**, 012309 (2010).
27. L. Cywiński, R. M. Lutchyn, C. P. Nave, S. Das Sarma, *Phys. Rev. B* **77**, 174509 (2008).
28. T. Gullion, D. Baker, M. S. Conradi, *J. Magn. Reson.* **89**, 479 (1990).
29. M. A. Nielsen, I. L. Chuang, *Quantum Computation and Quantum Information* (Cambridge Univ. Press, Cambridge, 2000).

30. We acknowledge support from the Defense Advanced Research Projects Agency, the Dutch Organization for Fundamental Research on Matter (FOM), and the Netherlands Organization for Scientific Research (NWO). Work at the Ames Laboratory was supported by the U.S. Department of Energy Basic Energy Sciences under contract DE-AC02-07CH11358.

Supporting Online Material

www.sciencemag.org/cgi/content/full/science.1192739/DC1
Materials and Methods
Figs. S1 to S5
References

24 May 2010; accepted 19 August 2010
Published online 9 September 2010;
10.1126/science.1192739
Include this information when citing this paper.

Multiple Exciton Collection in a Sensitized Photovoltaic System

Justin B. Sambur,[1,2] Thomas Novet,[3] B. A. Parkinson[1]*

Multiple exciton generation, the creation of two electron-hole pairs from one high-energy photon, is well established in bulk semiconductors, but assessments of the efficiency of this effect remain controversial in quantum-confined systems like semiconductor nanocrystals. We used a photoelectrochemical system composed of PbS nanocrystals chemically bound to TiO_2 single crystals to demonstrate the collection of photocurrents with quantum yields greater than one electron per photon. The strong electronic coupling and favorable energy level alignment between PbS nanocrystals and bulk TiO_2 facilitate extraction of multiple excitons more quickly than they recombine, as well as collection of hot electrons from higher quantum dot excited states. Our results have implications for increasing the efficiency of photovoltaic devices by avoiding losses resulting from the thermalization of photogenerated carriers.

The urgent need for massively scalable carbon-free energy sources has focused attention on both increasing the efficiency and decreasing the cost of photovoltaic cells. When electrons are excited by photons with energy (E_{hv}, where h is Planck's constant and v is photon frequency) in excess of a semiconductor band gap, they tend to rapidly thermally relax to the conduction band edge; in this context, Shockley and Queisser calculated the maximum solar to electrical energy conversion efficiency for an optimal single band gap (E_g) semiconductor absorber to be about 31% (*1*). Third-generation solar cells have their basis in concepts that can potentially circumvent the so-called Shockley-Queisser limit (*2*). One such mechanism currently under active investigation (*3*–*5*) is to convert the excess energy of incident photons with $E_{hv} \geq 2E_g$ into additional free carriers in the material. An ideal material would produce two carriers per photon beginning at $E_{hv} = 2E_g$ and additional carriers for photons with energies equal to multiples of E_g [i.e., for $E_{hv} = 4E_g$, four carriers are generated per photon; however, 94% of the maximum gain in power conversion efficiency would be produced with just two carriers per photon (*6*)]. This process is known as carrier multiplication via impact ionization in bulk semiconductors but is quite inefficient because it usually requires E_{hv} to be much greater than $2E_g$ to generate an additional carrier per incident photon. However, there have been suggestions (*7*, *8*) that the process could be more efficient in semiconductor nanocrystals or quantum dots (QDs) because of the electronic structure associated with carrier confinement in three dimensions. In QDs, the process is known as multiple exciton generation (MEG) because the carriers are not free but instead are correlated as a result of confinement. Optical measurements of various nanomaterial systems, including colloidal QD solutions (*9*–*17*), QD thin films (*18*), and single-walled carbon nanotubes (SWCNT) (*19*), have identified signatures of MEG, but the generation efficiency in nanomaterials relative to bulk materials is still under discussion (*20*–*22*).

Despite numerous reports of optical detection of MEG in QDs, multiple exciton collection (MEC) from QDs, converting absorbed photons into photocurrents with quantum yields greater than one, has not yet been observed in a photovoltaic device. Recent reports measured MEG photocurrent in individual SWCNT photodiodes operating at low temperatures (*23*), separation of

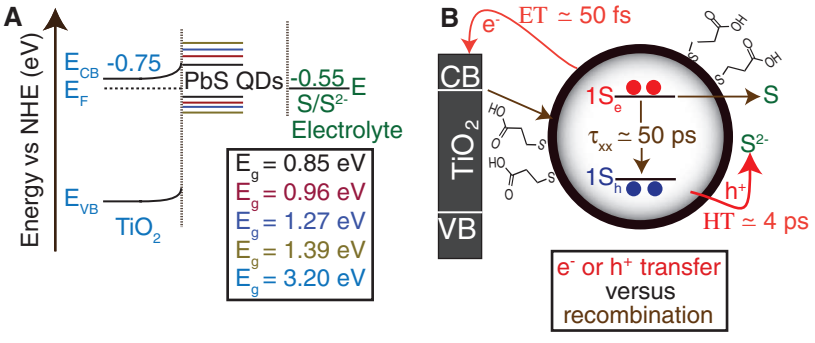

Fig. 1. Band energy diagram indicating the relevant energy levels and kinetic processes that describe PbS QD ET and HT into the TiO_2 conduction band and the sulfide/polysulfide electrolyte, respectively. (**A**) Energy-level alignment of the TiO_2 conduction band (*35*) with variously sized PbS QDs and the S/S^{2-} redox couple at pH 13. (Inset) The band gap energies of TiO_2 and the QDs used in this study. (**B**) Representation of a QD adsorbed on a TiO_2 single crystal and the approximate time scales for efficient ET and HT compared with the biexciton lifetime (τ_{xx}), as well as other possible recombination pathways. $1S_e$ and $1S_h$ refer to the first excited electron and hole state, respectively. Red and brown arrows indicate the favorable processes and the possible recombination pathways, respectively.

[1]Department of Chemistry and School of Energy Resources, University of Wyoming, Laramie, WY 80271, USA. [2]Department of Chemistry, Colorado State University, Fort Collins, CO 80523, USA. [3]Voxtel Incorporated, Beaverton, OR 97006, USA.

*To whom correspondence should be addressed. E-mail: bparkin1@uwyo.edu